



# Rapid initiation of cell cycle reentry processes protects neurons from amyloid- $\beta$ toxicity

Stefania Ippati<sup>a,b,1,2</sup>, Yuanyuan Deng<sup>a,1</sup>, Julia van der Hoven<sup>a</sup>, Celine Heu<sup>c</sup>, Annika van Hummel<sup>a</sup>, Sook Wern Chua<sup>a</sup>, Esmeralda Paric<sup>a</sup>, Gabriella Chan<sup>a</sup>, Astrid Feiten<sup>a</sup>, Thomas Fath<sup>a</sup>, Yazi D. Ke<sup>a</sup>, Nikolas K. Haass<sup>d,3</sup>, and Lars M. Ittner<sup>a,2,3</sup>

<sup>a</sup>Dementia Research Centre, Department of Biomedical Sciences, Faculty of Medicine Health and Human Sciences, Macquarie University, Sydney, NSW 2109, Australia; <sup>b</sup>San Raffaele Scientific Institute, San Raffaele Hospital, 20132 Milan, Italy; <sup>c</sup>Biomedical Imaging Facility, Mark Wainwright Analytical Centre, University of New South Wales, Sydney NSW 2052, Australia; and <sup>d</sup>The University of Queensland Diamantina Institute, The University of Queensland, Brisbane, QLD 4102, Australia

Edited by Pasko Rakic, Yale University, New Haven, CT, and approved February 16, 2021 (received for review June 17, 2020)

Neurons are postmitotic cells. Reactivation of the cell cycle by neurons has been reported in Alzheimer's disease (AD) brains and models. This gave rise to the hypothesis that reentering the cell cycle renders neurons vulnerable and thus contributes to AD pathogenesis. Here, we use the fluorescent ubiquitination-based cell cycle indicator (FUCCI) technology to monitor the cell cycle in live neurons. We found transient, self-limited cell cycle reentry activity in naive neurons, suggesting that their postmitotic state is a dynamic process. Furthermore, we observed a diverse response to oligomeric amyloid- $\beta$  (oA $\beta$ ) challenge; neurons without cell cycle reentry activity would undergo cell death without activating the FUCCI reporter, while neurons undergoing cell cycle reentry activity at the time of the oA $\beta$  challenge could maintain and increase FUCCI reporter signal and evade cell death. Accordingly, we observed marked neuronal FUCCI positivity in the brains of human mutant A $\beta$  precursor protein transgenic (APP23) mice together with increased neuronal expression of the endogenous cell cycle control protein geminin in the brains of 3-mo-old APP23 mice and human AD brains. Taken together, our data challenge the current view on cell cycle in neurons and AD, suggesting that pathways active during early cell cycle reentry in neurons protect from A $\beta$  toxicity.

Alzheimer | cell cycle | postmitotic neurons | FUCCI

Alzheimer's disease (AD) is the most prevalent of all the neurodegenerative disorders. Distinct protein inclusions, amyloid- $\beta$  (A $\beta$ ) plaques and neurofibrillary tangles (NFTs) characterize the AD brain (1). The exact causes of neuronal cell death in AD are still debated but several neuropathological studies have linked neuronal death to unexpected reappearance of cell cycle events (2–4). Accordingly, cell cycle activation, aberrant DNA replication, as well as aneuploidy have been found in neurons of AD brains (5–11). Furthermore, numbers of aneuploid neurons that are rare in control brains were increased in AD brains (5, 12, 13). However, mitosis itself has not been reported, and it appears that postmitotic neurons in AD patients cannot complete the cell cycle (14). In dividing cells, the coordination of the cell cycle requires interplay between cyclins and cyclin-dependent kinases (CDKs) at different checkpoints and the transitions between different phases are tightly regulated (15, 16). Therefore, it has been suggested that cell cycle reentry of differentiated mature neurons would have detrimental consequences, rendering them vulnerable and contribute to neurodegeneration (4, 8, 17). However, it remains unclear whether cell cycle events are a prerequisite for neuronal death, and why aneuploid neurons accumulate in AD brains.

The introduction of the fluorescent ubiquitination-based cell cycle indicator (FUCCI) system enabled live tracking of cell cycle progress in dividing cells (18) and has been valuable in understanding the implications of the cell cycle in disease pathogenesis, e.g., in cancer (19–21).

Briefly, the FUCCI system allows live monitoring of the cell cycle in cells, visualized by the ectopic expression of red and green fluorescent-tagged truncated proteins, mKO2-hCdt1 (30–120) and mAG-hGem (1–110), respectively, distinguishing the G1 from S, G2, and M phases (22). While frequently used in cancer and developmental biology research (23–25) to our knowledge, the FUCCI system has not been used to study mature neurons, including in the context of neurodegenerative diseases.

Here, we applied FUCCI to primary hippocampal neuronal cultures challenged with oligomeric A $\beta$  (oA $\beta$ ) and transgenic mice with expression of mutant human amyloid precursor protein (APP), which are both established models of AD (26–29). By obtaining quantitative and qualitative information about cell cycle events (CCEs) in response to A $\beta$ , we show that increased FUCCI reporter activity was associated with resistance to A $\beta$ -induced cell death, which is contrary to the current opinion of CCEs contributing to neurodegeneration in AD.

## Results

**Mature Neurons Undergo Transient, Self-Terminating Cell Cycle Reentry.** Cdt1 and Geminin are expressed during neurogenesis in development and in adult neuronal progenitors in the central

### Significance

The FUCCI reporter system allows live monitoring of the cell cycle via temporal expression of fluorescence markers of G0/1 or S/G2/M cell cycle phases. We found transient FUCCI reporter activity in naive neurons but not cell division, suggesting that the postmitotic state of neurons is rather a dynamic process of suppressing the cell cycle than a definite G0 state. Exposing neurons to amyloid- $\beta$  resulted in death of the majority of neurons without cell cycle contribution. A subset of neurons that entered early stages of cell cycle and maintained this state were protected from amyloid- $\beta$ -induced cell death. Consistently, we found high FUCCI reporter activity in the brains of mice that form amyloid- $\beta$  through transgenic expression of the amyloid- $\beta$  precursor protein.

Author contributions: S.I., Y.D., N.K.H., and L.M.I. designed research; S.I., Y.D., J.v.d.H., C.H., A.v.H., S.W.C., E.P., G.C., A.F., and T.F. performed research; S.I., Y.D., and Y.D.K. analyzed data; and S.I., Y.D., Y.D.K., N.K.H., and L.M.I. wrote the paper.

The authors declare no competing interest.

This article is a PNAS Direct Submission.

Published under the PNAS license.

<sup>1</sup>S.I. and Y.D. contributed equally to this work.

<sup>2</sup>To whom correspondence may be addressed. Email: stefania.ippati@hsr.it or lars.ittner@mq.edu.au.

<sup>3</sup>N.K.H. and L.M.I. contributed equally to this work.

This article contains supporting information online at <https://www.pnas.org/lookup/suppl/doi:10.1073/pnas.2011876118/-DCSupplemental>.

Published March 18, 2021.

nervous system (CNS) in a cell cycle phase-specific manner (30). Their expression is lost upon neuronal differentiation (30). Beyond this study, the use of the FUCCI system has been limited to nonneuronal cells (25, 31). To study CCE in live neurons, we first adapted the FUCCI reporter system to cultured primary hippocampal neurons (Fig. 1A). In order to achieve high (>90%) transfection efficacy in the primary neurons for subsequent quantitative analysis, we employed adeno-associated virus (AAV)-mediated transduction (32). For this, mKO2-hCdt1 (30-120) and mAG-hGem (1-110) were cloned individually into AAV vectors for neuronal expression driven by a synapsin promoter. Neuron specificity of the hSyn1 promoter and absence of expression in glial cells was confirmed *in vivo* (SI Appendix, Fig. S1). Following viral transduction with individual vectors at 7 d *in vitro* (DIV), we performed live cell imaging of primary hippocampal neurons for 48 h from 14 DIV followed by immunofluorescent staining. Cells were stained for neuronal markers NeuN,  $\beta$ 3-tubulin, and MAP2, to determine expression specificity of the neuronal human synapsin 1 (hSyn1) promoter used and efficacy of the FUCCI system (Fig. 1B and SI Appendix, Fig. S2). Very few neurons showed green fluorescence when transduced with mAG-hGem AAVs, while the vast majority of neurons fluoresced red when transduced with mKO2-hCdt1 AAVs. Accordingly, quantification showed that in 2-wk-old primary hippocampal neurons transduced with mKO2-hCdt1 AAVs, virtually all neurons ( $95 \pm 3.3\%$ ) imaged resided in G0/1 phase (mKO2+) (Fig. 1C and SI Appendix, Fig. S3 A and B). Surprisingly, only  $9.8 \pm 3.6\%$  of all neurons imaged were mAG positive (mAG+) when transduced with mAG-hGem AAVs (Fig. 1D and SI Appendix, Fig. S3 C and D). Treatment of mAG-hGem (1-110)-transduced neuron cultures with the proteasome inhibitor MG132 resulted in green fluorescence of all cells, confirming complete transduction efficacy (SI Appendix, Fig. S4 and Supporting Text). Simultaneous expression of mKO2-hCdt1 (30-120) and mAG-hGem (1-110) showed that nearly all mAG+ neurons were also mKO2+ (Fig. 1B), suggesting early S-phase processes in our neurons as observed when using the combined FUCCI reporter system in dividing cells (22). In line with these findings, no DNA synthesis and replication that typically occurs in the S phase of dividing cells was detected in mAG+ neurons (SI Appendix, Fig. S5). Live cell imaging of mKO2-hCdt1 (30-120) and mAG-hGem (1-110)-expressing cells showed transient green fluorescence in neurons that continue to express mKO2-hCdt1 (30-120) (Fig. 1E and Movie S1). This transient mAG positivity was self-limiting in all recorded cells and lasted for several hours only. The frequency of mAG positivity was consistent with numbers of mAG+ cells during end-point staining (Fig. 1C). It is noted that coexpression of mKO2-hCdt1 (30-120) and mAG-hGem (1-110) compromised neuronal long-term survival, in particular with the added stress of phototoxicity during live cell microscopy. Similar problems were observed when using both constructs together *in vivo* for brain expression where mice died prematurely. Therefore, we had to reduce AAV titers for mKO2-hCdt1 (30-120) expression when cotransducing with mAG-hGem AAVs, resulting in incomplete transduction of cultures and lower expression levels compared to cultures transduced with mKO2-hCdt1 AAVs alone and with higher titers (Fig. 1B, Bottom row). Accordingly, occasional mAG+ neurons without mKO2 expression are most likely due to lack of transduction from lower AAV mKO2-hCdt1 (30-120) titers (SI Appendix, Fig. S2). Expression of mAG-hGem (1-110) had no effect on cell survival during live cell microscopy or in mice. Hence, to monitor cell cycle reentry in neurons, we focus on the use of the FUCCI-S/G2/M reporter for the remainder of the study. To this end, mature postmitotic neurons transiently enter a state that resembles the early S phase of the cell cycle, which is self-limited to maintain the predominant G0 stage (Fig. 1F). We did not observe progression of cell cycle beyond early S-phase processes in cultured neurons.

**Reduced A $\beta$ -Induced Cell Death in Neurons Undergoing Cell Cycle Reentry.** Challenge of primary neurons with oA $\beta$  preparations is a frequently used model to study disease mechanisms in AD (28, 33). Accordingly, it has been reported that exposure of cultured wild-type (WT) neurons to oA $\beta$  caused cell cycle reentry and cell death (33, 34). To determine the dynamics of cell cycle reentry and its association with cell death we next challenged primary neurons that were transduced with mAG-hGem (1-110) with 0.5  $\mu$ M oA $\beta$  (SI Appendix, Fig. S6). To live track dying cells, we used in addition a fluorescent far red dye DRAQ7 (D7), which only passes membranes of compromised apoptotic cells, is not cytotoxic, and is therefore used for real-time cell death imaging (21, 35, 36). Forty-eight hours after exposure, oA $\beta$  induced a significant increase in mAG+ neurons ( $21.9 \pm 3.7\%$ ) compared to controls ( $9.7 \pm 2.5\%$ ) (Fig. 2 A–C), without induction of DNA synthesis and replication in these cells (SI Appendix, Fig. S5), indicative of early S-phase processes. Consistent with previous reports (37, 38), oA $\beta$  induced a significant and marked increase of D7+ dead neurons at 48 h (Fig. 2D). When assessing cell death, as measured by D7 uptake, in relation to mAG positivity, we found that oA $\beta$  induced only a small, yet significant, increase in D7+ cells with concomitant mAG fluorescence as compared to vehicle-treated controls that showed no mAG+/D7+ cells, while the vast majority of D7+ neurons showed no mAG fluorescence upon oA $\beta$  exposure (Fig. 2E and SI Appendix, Fig. S7). This suggests that oA $\beta$ -induced cell death and cell cycle activation were potentially distinct events under the current experimental conditions.

Finally, we addressed what distinguished D7+ from D7–neurons of the mAG+ population after oA $\beta$  challenge. Therefore, we traced mAG fluorescence intensity over the entire recording period in the two fractions of mAG+ neurons, mAG+D7– (Fig. 3A) and mAG+D7+ (Fig. 3B), following oA $\beta$  exposure. Considering these two mAG+ fractions, cells that did not undergo cell death showed a sharp and highly reproducible peak in mAG fluorescence shortly after oA $\beta$  exposure followed by a progressive increase over the entire recording period, resulting in an intense mAG fluorescence (Fig. 3C and E, green). In contrast, cells that eventually succumb to oA $\beta$  toxicity fail to increase mAG fluorescence quickly after the challenge, but instead show a slow increase followed by a decrease in mAG fluorescence levels within  $\sim 25$  h after oA $\beta$  treatment (Fig. 3C and E, red). Focusing on early states after oA $\beta$  exposure, we measured the fluorescence intensity of mAG at 3 h after exposure to oA $\beta$  (Fig. 3F). Levels of mAG fluorescence were different in the two fractions of neurons, mAG+D7– (A $\beta$ ) and mAG+D7+ (A $\beta$ ) as corroborated by the slope values of the regression lines (Fig. 3C and D). Neurons with high mAG fluorescence, 3 h after being exposed to oA $\beta$  survived at 48 h (i.e., showed no D7 uptake during the entire recording time). On the contrary, neurons with low mAG fluorescence underwent cell death. This suggests that the dynamics of cell cycle reactivation, i.e., rapid induction and sustained cell cycle processes, are critical for mediating the protective effects.

**Abundant Initiation of Cell Cycle Induction Processes in APP Mice and Human AD.** If increased cell cycle activity is indeed protecting cultured neurons from oA $\beta$  toxicity, we speculated to find similarly increased mAG positivity in brains of mice with high A $\beta$  levels but minimal cell loss. Therefore, we used AAV-mediated delivery of the mAG-hGem (1-110) reporter into the brains of APP23 mice and their nontransgenic (non-tg) littermates at birth (Fig. 4A). Using a synapsin promoter limited the expression of the FUCCI-S/G2/M reporter to neurons (SI Appendix, Fig. S1). APP23 mice express human KM670/771NL (Swedish) mutant APP under control of the murine Thy1 promoter in CNS neurons (29). APP23 mice show high A $\beta$  levels at young ages, present with premature mortality, develop memory deficits at 3 mo of age, and show plaque pathology starting from 6 mo of age (33, 39, 40). Furthermore,

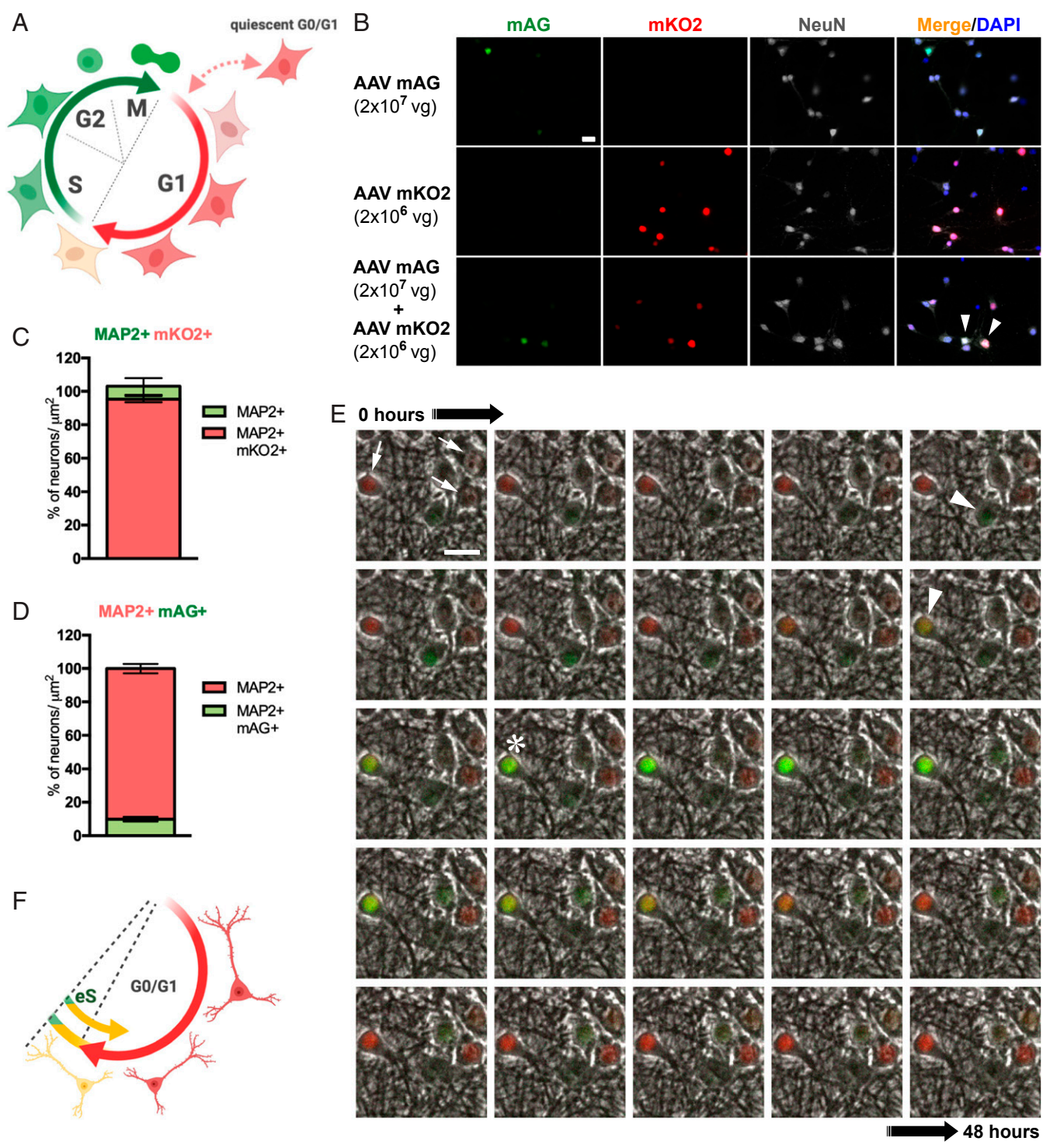


**Fig. 1.** Expression of FUCCI cell cycle reporters in mature hippocampal neurons. (A) Diagram of normal FUCCI cell cycle phase-specific fluorescent reporter activity during G0/G1 (red; mKO2) and S/G2/M phase (green; mAG) in dividing cells. (B) mKO2 (red) and mAG (green) fluorescence coimmunolabeled for the neuronal marker NeuN (white) of primary hippocampal neurons transduced with AAVs for mAG-hGem (1-110) (Top row), mKO2-hCdt1 (30-120) (Middle row), or combined mAG-hGem (1-110) and mKO2-hCdt1 (30-120) expression (Bottom row) at indicated AAV titers in parentheses (vg, viral genomes added to each culture). Arrowheads indicate cells with mKO2/mAG coactivity in merged images including nuclear DAPI staining (blue). (Scale bar, 20 μm.) (C) Numbers of MAP2 and mKO2+ neurons versus only MAP2+ cells (n = 5) in high-titer AAV mKO2-hCdt1-only transduced cells (SI Appendix, Fig. S3). Error bars indicate mean ± SEM. (D) Numbers of MAP2 and mAG+ neurons versus only MAP2+ cells (n = 7) in high-titer AAV mAG-hGem-only transduced cells. Error bars indicate mean ± SEM. (E) Image stack from 48-h recording of representative persisting mKO2 (red; arrows) and transient mAG expression (green; arrowheads) in vehicle-treated cultured hippocampal neurons. Note mKO2/mAG coactivity (yellow; asterisk) indicating transient early S phase processes while maintaining G0/G1 of postmitotic neurons. (Scale bar, 20 μm.) (F) Diagram of FUCCI reporter activity in postmitotic neurons maintaining G0/G1 (red; mKO2) and transiently engaging self-limiting early S phase (eS) processes (green; mAG) presenting as yellow from merged mKO2/mAG signals.

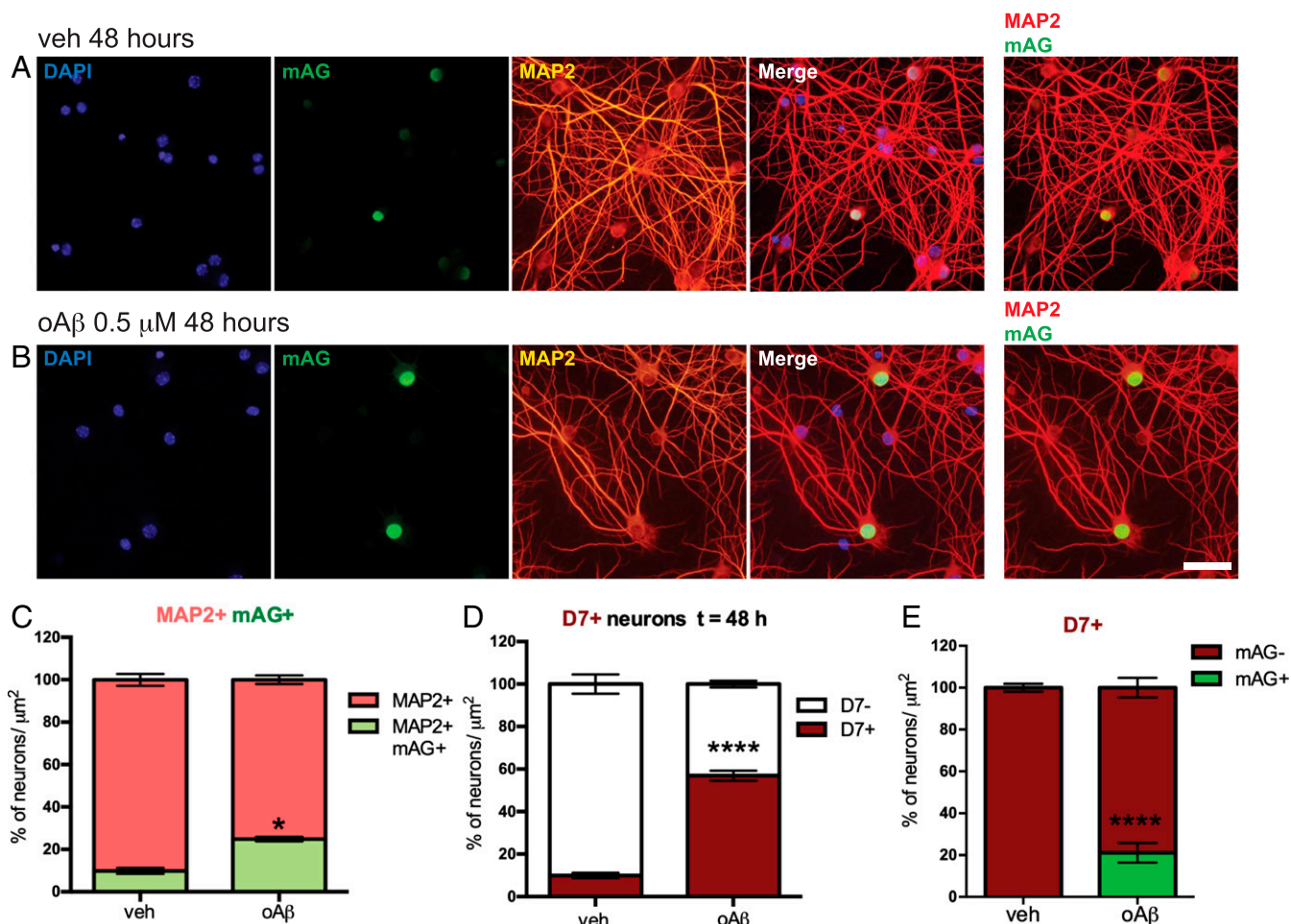


**Fig. 2.** oA $\beta$  induces cell death and cell cycle activation. (A and B) Representative images of mAG-hGem (1-110)-transduced neurons showing mAG fluorescence (green) costained for neuronal MAP2 (red) and nuclear DAPI (blue) 48 h after (A) vehicle or (B) 0.5  $\mu$ M oA $\beta$  challenge. Overlays of MAP2/mAG/DAPI (merge) and MAP2/mAG show colocalization. (Scale bar, 25  $\mu$ m.) (C) Fraction of MAP2 and mAG+ versus all MAP2+ oA $\beta$ - and vehicle-treated neurons ( $n = 7$  to 8; \* $P = 0.0213$ ; Student's  $t$  test). (D) Fraction of DRAQ7 (D7-) versus D7+, oA $\beta$ - and vehicle-treated neurons ( $n = 7$  to 8; \*\*\*\* $P < 0.0001$ ; Student's  $t$  test). (E) Fraction of mAG+ versus mAG- cells of all D7+ neurons after oA $\beta$  challenge or vehicle treatment ( $n = 8$ ; \*\*\*\* $P < 0.0001$ ; Student's  $t$  test).

we have previously reported presence of cell cycle markers in APP23 brains (41). Consistent with our data from non- and A $\beta$ -treated cultured neurons, quantitative analysis of serial 50- $\mu$ m brain sections revealed mAG fluorescence in the brains of both APP23 mice and non-tg littermates (Fig. 4B and *SI Appendix*, Fig. S8). However, numbers of mAG+ neurons were significantly higher in APP23 transgenic mice as compared with non-tg littermate brains (Fig. 4C). Similarly, mAG fluorescence intensity was significantly higher in APP23 brains, compared to non-tg mice at 3 mo of age (*SI Appendix*, Fig. S7). Furthermore, staining of APP23 brains with antibodies to geminin, a cell cycle marker of S/G2/M (22), showed markedly increased numbers of geminin-positive neurons as compared to non-tg brains, that showed only few geminin-positive neurons (Fig. 4D and E). Finally, consistent with our findings in APP23 mice, staining of human AD and non-demented control brains showed significantly increased numbers of geminin-positive neurons colabeled with NeuN in AD as compared to control brains (Fig. 4F and G). Taken together, presence of mAG-hGem (1-110) and infrequent neurons with endogenous geminin increase in non-tg mouse brain indicates that transient cell cycle reentry of postmitotic neurons happens naturally, while A $\beta$  expression is associated with increased mAG-hGem (1-110) activity and endogenous geminin increase in APP23 mouse and human AD brains.

## Discussion

In the present study, we show that naive postmitotic primary hippocampal neurons in culture transiently enter a state that resembles early stages of the cell cycle but efficiently limit this process to maintain the physiological G0/1 stage. This suggests dynamic rather than absolute maintenance of the postmitotic state of neurons. Furthermore, we found a dissociation between cell cycle reentry processes and cell death in neurons after exposure to A $\beta$ . Accordingly, neurons that showed rapid and persistent activation of the cell cycle process were protected from A $\beta$ -induced cell death within 48 h of live cell recording. In contrast, cells with only transient cell cycle activation succumbed to delayed death, while the vast majority of neurons dying after A $\beta$  exposure failed to reenter the cell cycle altogether. In line with our findings, we found increased numbers of neurons with high mAG reporter activity and high numbers of geminin-stained neurons in APP23 mice at ages without overt cell loss. Furthermore, human AD brains showed high numbers of geminin-positive neurons. Non-tg mice showed less mAG-hGem (1-110) reporter activity and sparse geminin staining of neurons, consistent with transient, self-limiting cell cycle reentry of subpopulations observed in cultured neurons.

Previous studies postulated that reentry of neurons into the cell cycle may constitute a common pathway leading to cell death in neurological diseases, including AD (42, 43). The role of the

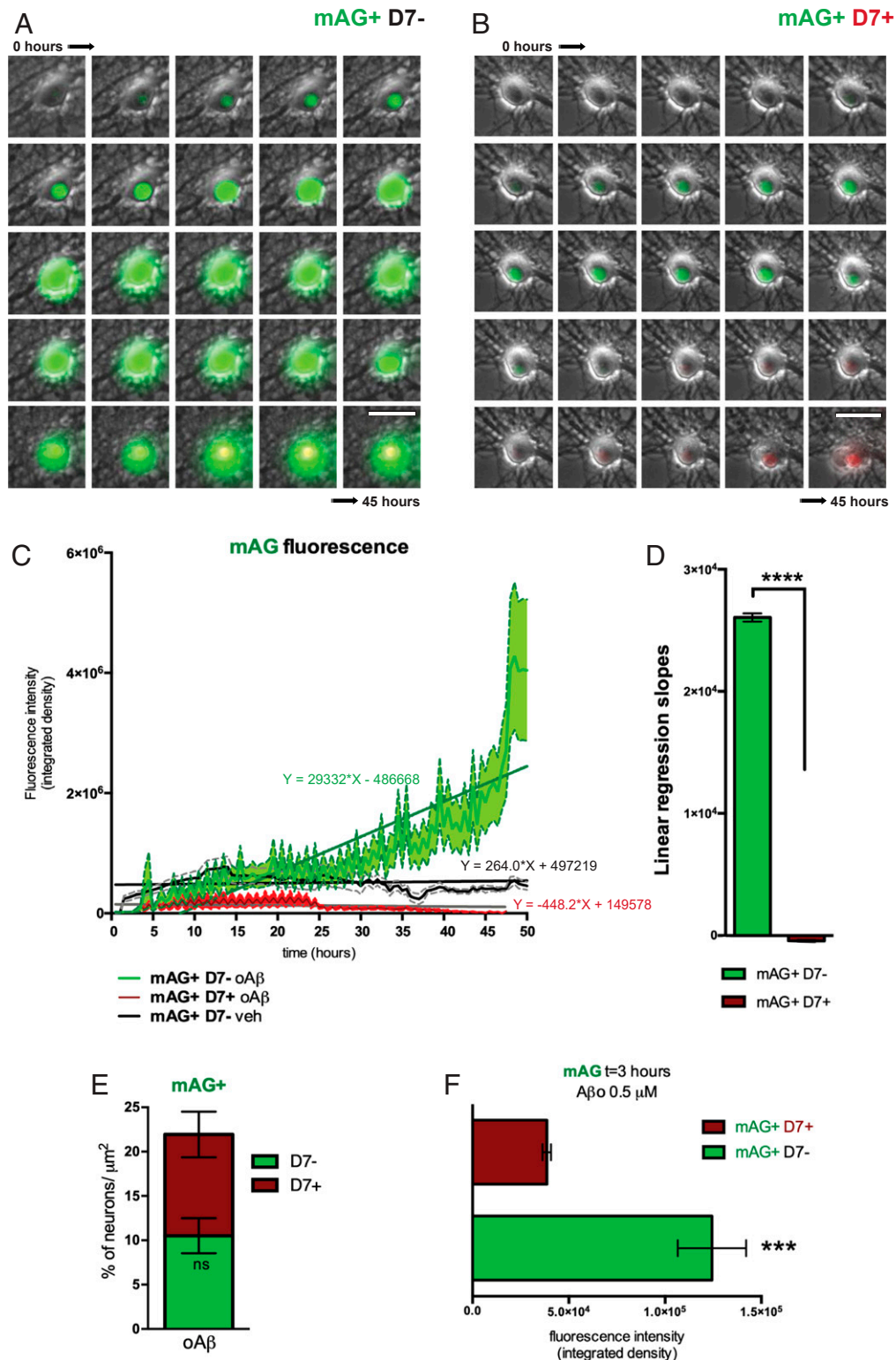


**Fig. 3.** Divergent neuronal cell cycle response to A $\beta$ . (A and B) Image stack from 45-h recording of representative mAG-hGem (1-110)-transduced cultured hippocampal neurons responding to A $\beta$  exposure by either (A) continually increasing mAG fluorescence intensity (mAG+; green) without DRAQ7 uptake (D7-), or (B) transient mAG fluorescence intensity followed by DRAQ7 uptake (D7+; red). (Scale bar, 25  $\mu\text{m}$ .) (C) Time course of mAG fluorescence intensity of mAG+/D7- (green) and mAG+/D7+ (red) neuronal populations upon 0.5  $\mu\text{M}$  oA $\beta$  exposure ( $n = 30$  to 37;  $P < 0.0001$ ; linear regression analysis). Transient mAG fluorescence trace of vehicle-treated neurons (black) is provided for comparison ( $n = 20 \pm 5$ ). Means  $\pm$  SEM are presented by the center trace and broken lines, respectively. (D) Comparison of mean linear regression slope values of mAG fluorescence intensity traces shown in C ( $n = 30$  to 37; \*\*\*\* $P < 0.0001$ ; Student's  $t$  test). (E) Area cell count comparison between mAG+/D7- and mAG+ D7+ oA $\beta$ -treated neurons ( $n = 8$ ; ns, not significant; Student's  $t$  test). (F) mAG fluorescence levels at 3 h after oA $\beta$  challenge in neurons classified as mAG+/D7- or mAG+/D7+ after 45 h of live imaging ( $n = 14$  to 24; \*\*\* $P = 0.0008$ ; Student's  $t$  test).

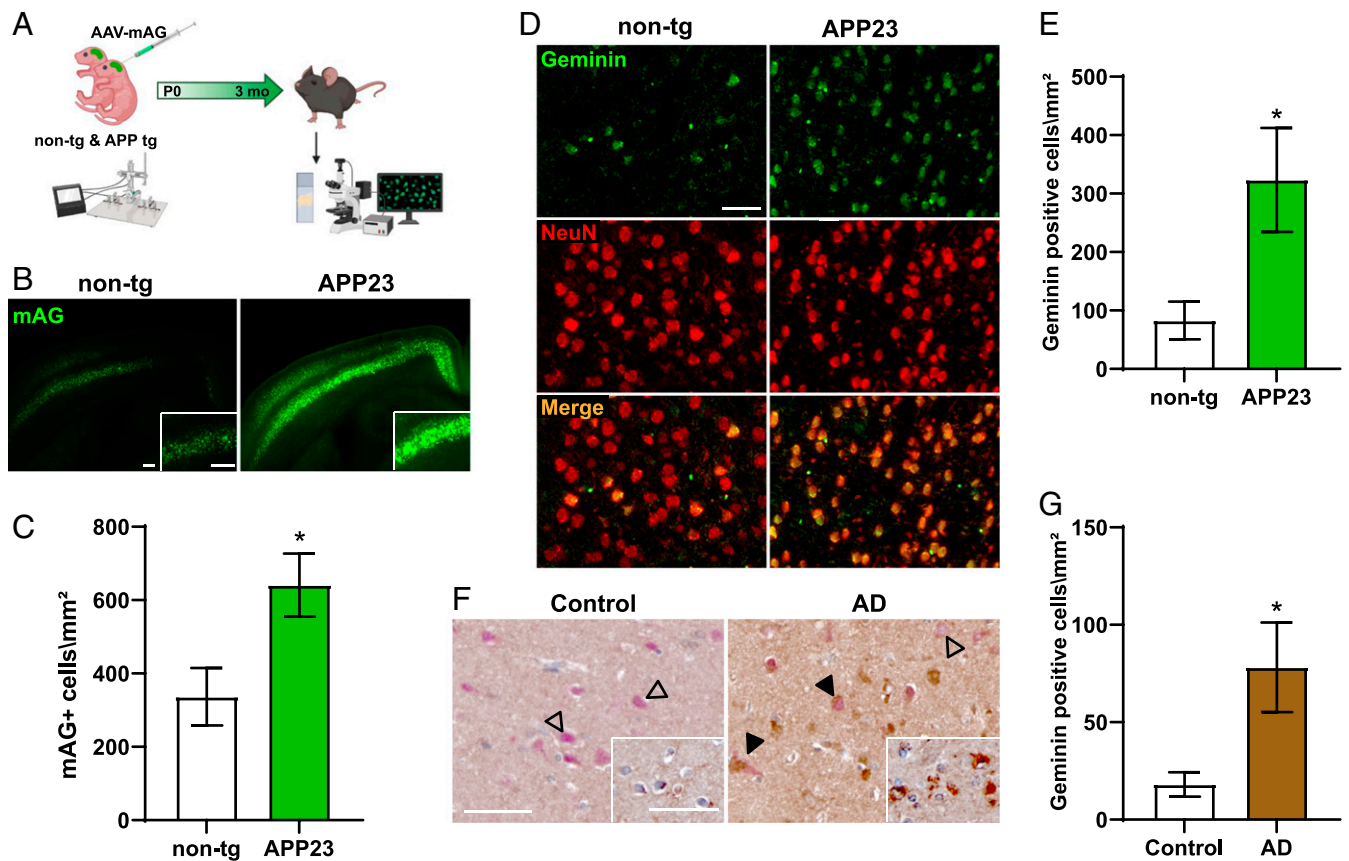


**Fig. 4.** Abundant cell cycle induction in mutant APP transgenic mice. (A) Experimental design for postnatal (P0) CNS delivery of AAV-mediated transduction of the FUCCI-S/G2/M reporter into the brains of APP23 mice and non-tg littermates; fluorescence of mAG in brains was imaged 3 mo later. (B) Representative fluorescence images of 50- $\mu\text{m}$ -thick brain sections from non-tg mice and APP23 littermates at 3 mo of age. (Insets) Higher-resolution images show layer IV/V in the cortex. (Scale bars, 200  $\mu\text{m}$ .) (C) Area cell density of mAG+ cells in non-tg and APP23 mice ( $n = 5$  to 10;  $*P = 0.0324$ ; Student's  $t$  test). (D) Representative immunofluorescence staining for endogenous geminin (green) and neuronal NeuN (red) of thin brain sections from 3-mo-old non-tg and APP23 mice. (Scale bar, 50  $\mu\text{m}$ .) (E) Area cell density of geminin-positive neurons in non-tg and APP23 brains ( $n = 4$  to 5;  $*P = 0.0269$ ; Student's  $t$  test). (F) Representative immunohistochemical (IHC) staining for geminin (brown; DAB) and NeuN (red; AP) AD and control (CTR) brain sections. Arrowheads: costaining of geminin and NeuN; open arrowheads: NeuN-stained neurons without geminin staining. (Inset) IHC of adjacent section for geminin only (brown; DAB). (Scale bars, 50  $\mu\text{m}$ .) (G) Area cell density of geminin-positive neurons in AD and CTR brains ( $n = 6$  each;  $*P = 0.0304$ ; Student's  $t$  test).

neuronal cell cycle is supported by data from AD patient brains that showed an increase in cell cycle protein expression (44–46). Similarly, exposure of cultured neurons to A $\beta$  or AD animal models induced cell cycle protein expression (34, 41, 43). Furthermore, AD brains are characterized by increased numbers of aneuploid neurons at autopsy (6, 13). However, converse evidence indicates that neurons can actively reenter cell cycle, replicate the DNA, and survive as tetraploid neurons during the course of different neurodegenerative diseases (42). Indeed, forced SV40 large T antigen (TAg)-mediated cell cycle reentry triggered hyperploidy and synaptic dysfunction but did not lead to apoptosis (47). Ultimately, to make the connection between A $\beta$ -induced cell cycle reentry and death, individual cell fate tracking would be required, but—to the best of our knowledge—had not been done before. Using the FUCCI cell cycle reporter system together with the cell death tracer DRAQ7 during live cell imaging we revealed that cells that reentered the cell cycle delayed or prevented A $\beta$ -induced death, in contrast to cells that fail to reenter or maintain the cell cycle. In line with these findings, we found markedly increased numbers of cells with mAG activity and expression of the endogenous S/G2/M protein geminin in A $\beta$ -forming APP23 mouse brains at a timepoint much earlier than previously reported for neuronal cell loss for this line. Moreover, it must be considered that the expression of cell cycle markers in degenerating postmitotic neurons may not follow the same

coordinated pattern as in proliferating cells (48–50). Accordingly, neurons becoming hyperploid in AD have been shown to undergo cell death only at late stages of disease progression (5), which is in line with our findings. Further supporting our data from cultured neurons and APP23 mice, we found significantly higher numbers of geminin-positive neurons in human AD brains as compared with nondemented controls. The abundance of geminin-positive neurons in AD in our study compared with previously reported numbers of aneuploid neurons in AD (6, 13), may suggest that induction of early cell cycle processes (i.e., early S phase) described by us are a common response to A $\beta$  toxicity, while true progression of neurons into later stages of the cell cycle with DNA amplification remains a rare event. Taken together our data suggest that cell cycle reentry and neuronal death are disconnected or even opposing events in AD.

Normal progression through the cell cycle is executed by the ubiquitin proteasome system (UPS), consisting of sets of enzymes that target substrates for proteasomal degradation of polyubiquitinated proteins (51, 52). Specifically, the multisubunit E3 ubiquitin ligase APC/C-Cdh1 targets multiple cell cycle-promoting cyclin-Cdk complexes including CDK2/cyclin E, CDK2/cyclin A, CDK4/cyclin D, and CDK6/cyclin D and the DNA replication components Cdt1 and Geminin for proteasomal degradation (53, 54), while at the same time maintaining levels of cell cycle inhibitor complexes p27Kip1 and p21Cip1 high (55, 56). An increase

in APC/CCdh1 activity has been observed during terminal neuronal differentiation (57, 58). Thus, dysregulation of the cell cycle machinery in AD might involve a dysfunctional APC/C-Cdh1 complex (59). Alternatively, generally impaired UPS function in AD (60, 61) may result in accumulation of cell cycle proteins. However, this would neither explain why only a subpopulation of cells showed increased mAG-hGem (1-110) nor its temporal profile when comparing  $\alpha\beta$ - and MG-132-treated neurons. APC/CCdh1 has been proposed to block postmitotic differentiated neurons from inappropriate cycling followed by apoptosis (58, 62). On the contrary, our study suggests that cell cycle progression in neurons does not lead to cell death. Using live imaging, we show that neurons with rapid and persistent S/G2/M-phase activation after  $\alpha\beta$  exposure virtually never died within the recording time. In contrast, neurons with delayed  $\alpha\beta$ -induced FUCCI-S/G2/M activation eventually succumb to neuronal death, although at a later timepoint when compared to the majority of cells that failed to induce the cell cycle at all and frequently died after  $\alpha\beta$  exposure. This is in line with a report showing that irradiated retinal pigment epithelial cells that failed to recover in response to DNA damage rapidly lost the G2 cell cycle protein Cyclin B1, while cells that eventually survived maintained Cyclin B1 at high levels (63). Our data suggest that the decision to execute apoptosis following  $\alpha\beta$  insult is established depending on the G2 cell cycle state beyond a specific threshold. Hence, we have identified a cell fate decision point related to cell cycle, in postmitotic neurons responding to  $\beta$  toxicity (*SI Appendix, Fig. S9*). Neurons with rapid and persistent  $\beta$ -induced cell cycle activation appear to have adopted a state that protected them from death, while cells that failed to induce persistent cell cycle states, possibly due to similar molecular mechanisms that self-limit physiological cell cycle activation in naive cells, were vulnerable to  $\beta$ . Which molecular pathways drive this heterogenic fate decision in response to  $\beta$  remain to be shown. One possibility is that accumulation of cell cycle checkpoint proteins inhibit proapoptotic pathways (64). Accordingly, cancer studies reported cyclins as powerful suppressors of cellular senescence (65). Constitutive Cyclin D1 production in B cells delays commitment to apoptosis by inducing Hsp70 chaperoning activity on proapoptotic factors (66). In quiescent hematopoietic stem and progenitor cells, D cyclins inhibit the expression of the death receptor Fas and its ligand, FasL, repressing apoptosis (67). Cyclin G negatively regulates the stabilization of p53 family proteins involved in promoting apoptosis or senescence (68, 69). Recent introduction of advanced FUCCI reporters for more accurate cell cycle phase analysis may provide new opportunities for future studies and further dissection of the early S phase processes of neurons (70–72). However, whether the newer-generation FUCCI reporters overcome the limitations of mKO2 and allow detailed monitoring of all cell cycle phases in mature neurons including *in vivo* remains to be shown.

In summary, our data suggest that the postmitotic state of neurons is a dynamic process, and naive neurons have to actively reverse spontaneous cell cycle reentry processes of the very early S phase rather than persisting in a passive permanent G0 state. Accordingly, we found naive neurons showing transient mAG positivity in primary neurons and in brains of naive mice displaying sparsely distributed neurons with high levels of the S/G2/M cell cycle protein geminin. Our observations of cell cycle pathway activities in naive neurons might have to be considered when studying processes of adult neurogenesis. To this end, we propose that rapid induction of pathways that lead to cell cycle reentry in response to  $\beta$  may protect neurons and prevent or delay cell death in AD. This may explain why increased and not less aneuploid neurons are present in AD brains at autopsy (6). To this end, our study warrants rethinking of the dynamics of CCEs in living neurons and their contribution to the pathogenesis of AD.

## Material and Methods

**Adeno-associated Viruses.** FUCCI cloning vectors were purchased from Amalgaam: pFUCCI-G1 Orange cloning vector (AM-V9001) encoding for the orange probe Kusabira-Orange2 fused to truncated human Cdt1 [mKO2-hCdt1 (30-120)] and pFUCCI-S/G2/M Green cloning vector (AM-V9014) encoding for the green probe Azami-Green1 fused to truncated human Geminin [mAG-hGem (1-110)]. For cell culture experiments, FUCCI vectors were cloned separately into pAM hSyn1-c-WPRE-bGHpA AAV plasmid and adeno-associated viruses produced as previously described (32, 73). The vector genome copy number (VG) was determined by qPCR using Brilliant III Ultra-Fast SYBRgreen qPCR Master Mix (600882, Stratagene). For stereotaxic injections, packaging of AAV-PHP.B-hSyn-pFucci-S/G2/M Green hmAG1 vector was performed as described previously (74). Titers were determined by qPCR.

**Primary Neuronal Cell Culture.** Culturing of primary embryonic mouse hippocampal neurons was performed as previously described (75). Briefly, sterile glass coverslips (12-mm diameter) placed into the central 8 wells of a 24-well culture plate, were coated with poly-D-lysine (PDL)-coating solution (0.1 mg/mL poly-D-lysine in borate buffer (50 mM boric acid, 23.6 mM sodium tetraborate). PDL-coated plates were left overnight in a 37 °C/5% CO<sub>2</sub> incubator. The following day, the coverslips were washed twice with sterile water. To generate primary neuronal cultures, time-pregnant C57BL/6 female mice were killed at gestational day E16.5. The E16.5 embryos were removed from the uterus and kept in ice-cold Hanks' balanced salt solution (HBSS). The brains and meninges were removed using curved forceps and the hippocampi were excised with microscissors and the fimbria along the concave side of each hippocampus removed to reduce astrocyte contamination. The hippocampi were transferred into fresh HBSS and then incubated with trypsin (Sigma) for 15 min at 37 °C. The 10 mg/mL stocks of DNase I (Sigma) were then added to the tissue at a final concentration of 1 mg/mL to digest precipitated DNA, for 30 s. The digested tissue was then washed twice with Dulbecco's modified Eagle medium containing 10% (vol/vol) heat-inactivated fetal bovine serum (plating medium). Subsequently, the tissue was slowly triturated using both wide and narrow fire-polished glass pipettes (Livingstone) to obtain homogenous cell suspensions. Cells were incubated for 2 h at 37 °C to allow them to attach to the PDL-coated surface. The plating medium was then removed and replaced with serum-free Neurobasal medium containing 2% (vol/vol) B27 supplement and 0.5 mM Glutamax. The cells were then allowed to mature for 10 d before being used in experiments. All cell culture media and reagents were supplied by Invitrogen. AAV FUCCI mKO2-hCdt1 (30-120) and AAV FUCCI mAG-hGem (1-110) were thawed and administered separately directly into the cell medium to 10-d-old primary WT hippocampal neurons. Transduction of primary neurons was done by adding  $2 \times 10^6$  to  $2 \times 10^7$  viral genomes (vg) to the cell culture medium, which is equivalent to multiplicity of infection (MOI) 30 and 300 vg/cell (MOI = multiplicity of infection = number of viral genome per cell) at the cell density used. Four days after AAV transduction, 2-wk-old primary neurons were incubated for 48 h with oligomeric  $\beta_{1-42}$  at 0.5  $\mu$ M. Controls were treated with the same amount of dimethyl sulfoxide (DMSO).

**Preparation of  $\beta_{1-42}$  Oligomers.** Lyophilized synthetic  $\beta_{1-42}$  (Bachem), was resuspended as previously described (76). Briefly, samples were dissolved in 1,1,1,3,3,3-hexafluoro-2-propanol (Sigma-Aldrich) to 1 mM, which was evaporated overnight at room temperature. The dried powder was resuspended in DMSO at 5 mM and sonicated for 10 min in a water bath. The peptide was then diluted to 100 mM in Neurobasal medium and incubated overnight at 4 °C, to prepare ( $\beta_{1-42}$  oligomers [ $\alpha\beta$ ]).  $\alpha\beta$  were added to primary neuron cultures in Neurobasal medium containing 2% (vol/vol) B27 supplement and 0.5 mM Glutamax at a final concentration of 0.5  $\mu$ M. Characterization of  $\alpha\beta$  was performed using atomic force microscopy and Western blot analysis (*SI Appendix, Fig. S6*) as described previously by Stine et al. (76). Controls were treated with the same concentration of DMSO diluted in Neurobasal medium.

**Atomic Force Microscopy.** Characterization of the  $\alpha\beta$  by atomic force microscopy was carried out at the Biomedical Imaging Facility of the University of New South Wales. Topography imaging was obtained using 50  $\mu$ L of sample spotted on freshly cleaved mica. After incubation of the mica at room temperature for 10 min, the sample was rinsed with ultrapure water and let dry for 15 min. The 2- $\mu$ m scan-size images were acquired on the Bioscope catalyst in PeakForce Tapping mode with a scanasyst air probe (0.4 N/m) in the height (topography) channel.

**Western Blotting.** Western blotting analysis has been performed as previously described (77, 78). In this study, 5 mM oligomeric  $\beta$  unheated samples

diluted in water were applied to 12% sodium dodecyl-sulfate polyacrylamide gel electrophoresis gels at 100 V for 90 min. Samples were subsequently electrophoretically transferred onto nitrocellulose membranes (GE Healthcare) in a Trans-BlotTM Turbo Transfer System (Bio-Rad) at 2.5 Amp constant up to 25 V for 10 min. Membranes were blocked in 5% nonfat dry milk in Tris-buffered saline (TBS) containing 0.0625% Tween-20 as described previously (79). Blots were incubated in the primary anti amyloid- $\beta$  antibody (mouse monoclonal anti amino acids 1 to 16 of  $\beta$ -amyloid, Bio Legend 803015) diluted in 5% nonfat dry milk in Tris-buffered saline containing 0.0625% Tween-20 overnight at 4 °C while shaking. The following day, the primary antibody was removed, and the membranes washed three times with TBS-T. The washed membranes were then incubated with a mouse horseradish peroxidase (HRP) coupled secondary antibody in 1% (wt/vol) bovine serum albumin (BSA)/TBS-T for 1 h at room temperature. Protein bands were visualized with Immobilon Western Chemiluminescent HRP Substrate (Millipore).

**Cell Live Imaging and Video Processing.** Directly following treatment with oA $\beta$ , cells were moved into a preheated stage-top incubator maintained at 37 °C/5% CO<sub>2</sub>, of an OLYMPUS IX83 (DP80) live cell microscope, fitted with an electron multiplying CCD camera or ZEISS Axio Observer. Primary neurons were imaged once every hour using a 20 $\times$  magnification objective, using multichannel (phase contrast, 488 GFP, 565/585 far red) Z-stack across multiple sample positions. The far-red fluorescent dye (DRAq7, Abcam), was added at the concentration of 3  $\mu$ M, 24 h after imaging. Cells were then imaged for other 20 to 24 h and image stacks processed by cellSens Dimension software (Olympus). All biological and technical replicates were performed using the same microscope acquisition and exposition settings (phase contrast 125 ms, GFP 142.9 ms, far red 137.9 ms). Videos were analyzed using Fiji ImageJ (NIH). To quantify fluorescence levels in live imaged cells, raw image stacks were digitalized, single cells selected, and fluorescence measured as integrated density values.

**Immunofluorescence Staining and Cell Counting.** Immunofluorescence staining was performed as previously described (80). Briefly, cells were fixed with prewarmed 4% (wt/vol) paraformaldehyde in phosphate-buffered saline (PBS) for 10 min at room temperature and then washed three times with PBS. The coverslips were removed from the culture plate and placed on ParafilmTM in a humidified chamber. The cells were then permeabilized with 0.2% (vol/vol) Nonidet P-40 (Fluka) in PBS for 5 min and then incubated in blocking buffer (3% [wt/vol] heat-inactivated normal goat serum, 2% (wt/vol) BSA, 0.1% Tween-20 in PBS) for 1 h at room temperature. Primary antibodies (mouse monoclonal anti-MAP2, Sigma M9942; mouse monoclonal anti-NeuN, Merck Millipore MAB377; chicken polyclonal anti-MAP2, Abcam ab5392; chicken polyclonal anti- $\beta$ -tubulin, Merck Millipore AB9354) were appropriately diluted in blocking buffer, added to the coverslip, and left overnight at 4 °C. The following day the coverslips were washed three times with PBS and incubated for 1 h at room temperature with secondary fluorescent antibodies and DAPI staining. The coverslips were mounted onto glass slides using ProLong Gold antifade reagent (Life Technologies) and dried for 24 h at room temperature before imaging. Cell counting was performed as described previously (77, 81). Briefly, following fixation and staining, neurons were quantified counting from four different random areas of the coverslip. Images were captured at 20 $\times$  or 40 $\times$  magnification with an Olympus BX51 microscope equipped with a DP70 CCD camera or the Zeiss AxioImager.Z1, background-subtracted, digitized, and processed by means of Fiji ImageJ image processing software (NIH).

**Mice.** APP23 mice have been previously described (29). Briefly, an expression construct containing a murine Thy-1 promoter was used to drive neuron-specific expression of human mutated APP751 (Swedish double mutation 670/671 KM $\rightarrow$ NL) in C57BL/6 mice. Mice were maintained on a C57BL/6 background. Transgenic mice were identified by PCR. Strains were established from founder mice and backcrossed eight times onto the C57BL/6 background. All experiments have been approved by the Animal Ethics Committee of the

University of New South Wales. For AAV-mediated delivery of the mAG-hGem (1-110), AAV-PHP.B-hsyn-pFucci-S/G2/M Green mAG ( $1 \times 10^{13}$  viral genomes/mL) was injected at four sites (1.5  $\mu$ L/site) bilaterally into the brains of cryoanesthetized neonatal mice as described (82) to APP23 mice and non-tg littermates. All mice were killed for analysis at 3 mo of age followed by PBS perfusion. Brains for stainings were processed in an Excelsior tissue processor (Thermo) and paraffin embedded, while brains from AAV-injected mice were sectioned to 50  $\mu$ m with Vibratome and imaged on a Zeiss Axio Scan.Z1 fluorescence scanner; the number and intensity of mAG+ cells were analyzed by Fiji ImageJ (NIH). Quantification of fluorescence was performed as previously described (81, 83).

**Human Brain Tissue.** Postmortem human brain tissue sections from donors diagnosed with the AD ( $n = 6$ ) and age-matched nondemented controls ( $n = 6$ ) were obtained from the New South Wales Brain Bank. For all brain tissue, clinical and pathological information was obtained with written consent from the brain donors and their next of kin as approved by the Human Ethics Committees of the South Eastern and Illawarra Area Health Service, the University of New South Wales, and the University of Sydney. All procedures complied with the statement on human experimentation issued by the National Health and Medical Research Council of Australia. The average age at death ( $\pm$ SD) was as follows: AD, 70  $\pm$  6 y and for age-matched nondemented controls, 70  $\pm$  7 y. The average disease duration ( $\pm$ SD) was 7  $\pm$  3 y for AD cases. None of the cases had a family history suggestive of an autosomal dominant disease.

**Immunohistochemistry.** Brain sections from mice and human patients were deparaffinated, rehydrated, and blocked, followed by overnight incubation at 4 °C with primary antibody: mouse monoclonal anti-EGFP (Abcam ab184601); mouse monoclonal anti-NeuN (Merck Millipore MAB377); chicken polyclonal anti-NeuN (Merck Millipore ABN91); rabbit monoclonal anti-NeuN (Abcam ab184601); chicken polyclonal Anti-MAP2 (Abcam ab5392); rabbit polyclonal Anti-IBA-1 (Wako WEE4506); mouse monoclonal Anti-GFAP (Sigma G3893); rabbit polyclonal anti-geminin (Proteintech 10802-1-AP). After washing with PBS, secondary antibodies (goat anti-mouse/rabbit/chicken conjugated to Alexa 488, 555, 568, or 647 dyes) were used with or without addition of DAPI for 1 h at room temperature for immunofluorescence staining. Mouse or rabbit-biotinylated secondary antibodies and avidin-biotin complex horseradish peroxidase (HRP) or alkaline phosphatase (AP) detection kit were applied for chromogenic detection. Stainings were imaged using the AxioScan.Z1 slide scanner and analyzed within Fiji ImageJ image processing software (NIH).

**Statistical Analysis.** Statistical analysis was performed using GraphPad Prism version 6.0. Student's  $t$  tests were performed for pairwise comparison. Linear regression and correlation analysis were done by sum-of-squares minimization. All values are presented as mean  $\pm$  SEM. Details on individual test parameters and  $n$  numbers are provided in figure legends.

**Schematic Design.** Schematics and diagrams were generated with BioRender software and Adobe Illustrator.

**Data Availability.** All study data are included in the article and/or supporting information.

**ACKNOWLEDGMENTS.** We thank Dr. Sandra Fok and Dr. Arthur Chien for technical assistance with the live cell microscope. We thank Yijun Lin for production of adeno-associated viruses. We thank Holly Stefan for primary neuron preparations. We thank Prof. Brian Gabrielli (Mater Research Institute, Brisbane), Dr. Mathew Jones (University of Queensland Diamantina Institute, Brisbane), and Dr. Mark Adams (Queensland University of Technology, Brisbane) for their thoughtful comments on the manuscript. We also thank the animal facility staff for caring for our mouse colonies. This work was supported by the National Health and Medical Research Council (Grants 1081916, 1123564, 1132524, 1136241, and 1143848) and the Australian Research Council (Grant DP150104321).

1. H. W. Querfurth, F. M. LaFerla, Alzheimer's disease. *N. Engl. J. Med.* **362**, 329–344 (2010).
2. J. Busser, D. S. Geldmacher, K. Herrup, Ectopic cell cycle proteins predict the sites of neuronal cell death in Alzheimer's disease brain. *J. Neurosci.* **18**, 2801–2807 (1998).
3. J. J. Hoozemans et al., Cyclin D1 and cyclin E are co-localized with cyclo-oxygenase 2 (COX-2) in pyramidal neurons in Alzheimer disease temporal cortex. *J. Neuropathol. Exp. Neurol.* **61**, 678–688 (2002).
4. Y. Yang, E. J. Mufson, K. Herrup, Neuronal cell death is preceded by cell cycle events at all stages of Alzheimer's disease. *J. Neurosci.* **23**, 2557–2563 (2003).

5. T. Arendt, Cell cycle activation and aneuploid neurons in Alzheimer's disease. *Mol. Neurobiol.* **46**, 125–135 (2012).
6. B. Mosch et al., Aneuploidy and DNA replication in the normal human brain and Alzheimer's disease. *J. Neurosci.* **27**, 6859–6867 (2007).
7. T. Arendt, B. Mosch, M. Morawski, Neuronal aneuploidy in health and disease: A cytomic approach to understand the molecular individuality of neurons. *Int. J. Mol. Sci.* **10**, 1609–1627 (2009).
8. T. Arendt, M. Holzer, U. Gärtner, M. K. Brückner, Aberrancies in signal transduction and cell cycle related events in Alzheimer's disease. *J. Neural. Transm. Suppl.* **54**, 147–158 (1998).



9. W. K. Liu, R. T. Williams, F. L. Hall, D. W. Dickson, S. H. Yen, Detection of a Cdc2-related kinase associated with Alzheimer paired helical filaments. *Am. J. Pathol.* **146**, 228–238 (1995).
10. T. W. Smith, C. F. Lippa, Ki-67 immunoreactivity in Alzheimer's disease and other neurodegenerative disorders. *J. Neuropathol. Exp. Neurol.* **54**, 297–303 (1995).
11. A. McShea, P. L. Harris, K. R. Webster, A. F. Wahl, M. A. Smith, Abnormal expression of the cell cycle regulators p16 and CDK4 in Alzheimer's disease. *Am. J. Pathol.* **150**, 1933–1939 (1997).
12. B. E. Ward, R. H. Cook, A. Robinson, J. H. Austin, Increased aneuploidy in Alzheimer disease. *Am. J. Med. Genet.* **3**, 137–144 (1979).
13. C. E. Shepherd, Y. Yang, G. M. Halliday, Region- and cell-specific aneuploidy in brain aging and neurodegeneration. *Neuroscience* **374**, 326–334 (2018).
14. L. A. van Leeuwen, J. J. Hoozemans, Physiological and pathophysiological functions of cell cycle proteins in post-mitotic neurons: Implications for Alzheimer's disease. *Acta Neuropathol.* **129**, 511–525 (2015).
15. M. Hengstschläger, K. Braun, T. Soucek, A. Miloloz, E. Hengstschläger-Ott, Cyclin-dependent kinases at the G1-S transition of the mammalian cell cycle. *Mutat. Res.* **436**, 1–9 (1999).
16. R. P. Fisher, The CDK network: Linking cycles of cell division and gene expression. *Genes Cancer* **3**, 731–738 (2012).
17. A. McShea, A. F. Wahl, M. A. Smith, Re-entry into the cell cycle: A mechanism for neurodegeneration in Alzheimer disease. *Med. Hypotheses* **52**, 525–527 (1999).
18. R. H. Newman, J. Zhang, Fucci: Street lights on the road to mitosis. *Chem. Biol.* **15**, 97–98 (2008).
19. K. A. Beaumont *et al.*, Cell cycle phase-specific drug resistance as an escape mechanism of melanoma cells. *J. Invest. Dermatol.* **136**, 1479–1489 (2016).
20. N. K. Haass *et al.*, Real-time cell cycle imaging during melanoma growth, invasion, and drug response. *Pigment Cell Melanoma Res.* **27**, 764–776 (2014).
21. M. P. Smith *et al.*, Targeting endothelin receptor signalling overcomes heterogeneity driven therapy failure. *EMBO Mol. Med.* **9**, 1011–1029 (2017).
22. A. Sakaue-Sawano *et al.*, Visualizing spatiotemporal dynamics of multicellular cell cycle progression. *Cell* **132**, 487–498 (2008).
23. K. A. Beaumont, A. Anfoso, F. Ahmed, W. Weninger, N. K. Haass, Imaging- and flow cytometry-based analysis of cell position and the cell cycle in 3D melanoma spheroids. *J. Vis. Exp.*, e53486 (2015).
24. A. M. Singh, R. Trost, B. Boward, S. Dalton, Utilizing FUCCI reporters to understand pluripotent stem cell biology. *Methods* **101**, 4–10 (2016).
25. L. Spoerri, K. A. Beaumont, A. Anfoso, N. K. Haass, Real-time cell cycle imaging in a 3D cell culture model of melanoma. *Methods Mol. Biol.* **1612**, 401–416 (2017).
26. D. M. Walsh *et al.*, Naturally secreted oligomers of amyloid beta protein potently inhibit hippocampal long-term potentiation in vivo. *Nature* **416**, 535–539 (2002).
27. J. Hardy, D. J. Selkoe, The amyloid hypothesis of Alzheimer's disease: Progress and problems on the road to therapeutics. *Science* **297**, 353–356 (2002).
28. T. Oda *et al.*, Clusterin (apoJ) alters the aggregation of amyloid beta-peptide (A beta 1–42) and forms slowly sedimenting A beta complexes that cause oxidative stress. *Exp. Neurol.* **136**, 22–31 (1995).
29. C. Sturchler-Pierrat *et al.*, Two amyloid precursor protein transgenic mouse models with Alzheimer disease-like pathology. *Proc. Natl. Acad. Sci. U.S.A.* **94**, 13287–13292 (1997).
30. M. Spella *et al.*, Licensing regulators Geminin and Cdt1 identify progenitor cells of the mouse CNS in a specific phase of the cell cycle. *Neuroscience* **147**, 373–387 (2007).
31. N. Zielke, B. A. Edgar, FUCCI sensors: Powerful new tools for analysis of cell proliferation. *Wiley Interdiscip. Rev. Dev. Biol.* **4**, 469–487 (2015).
32. X. Huang *et al.*, AAV2 production with optimized N/P ratio and PEI-mediated transfection results in low toxicity and high titer for in vitro and in vivo applications. *J. Virol. Methods* **193**, 270–277 (2013).
33. A. Ittner *et al.*, Site-specific phosphorylation of tau inhibits amyloid- $\beta$  toxicity in Alzheimer's mice. *Science* **354**, 904–908 (2016).
34. M. E. Seward *et al.*, Amyloid- $\beta$  signals through tau to drive ectopic neuronal cell cycle re-entry in Alzheimer's disease. *J. Cell Sci.* **126**, 1278–1286 (2013).
35. A. Kienzle *et al.*, Dendritic mesoporous silica nanoparticles for pH-stimuli-responsive drug delivery of TNF- $\alpha$ . *Adv. Healthc. Mater.* **6**, 1700012 (2017).
36. E. F. Lee *et al.*, BCL-XL and MCL-1 are the key BCL-2 family proteins in melanoma cell survival. *Cell Death Dis.* **10**, 342 (2019).
37. I. Kuperstein *et al.*, Neurotoxicity of Alzheimer's disease A $\beta$  peptides is induced by small changes in the A $\beta$ 42 to A $\beta$ 40 ratio. *EMBO J.* **29**, 3408–3420 (2010).
38. R. Kaye, C. A. Lasagna-Reeves, Molecular mechanisms of amyloid oligomers toxicity. *J. Alzheimers Dis.* **33** (suppl. 1), S67–S78 (2013).
39. L. M. Ittner *et al.*, Dendritic function of tau mediates amyloid-beta toxicity in Alzheimer's disease mouse models. *Cell* **142**, 387–397 (2010).
40. A. A. Ittner, A. Gladbach, J. Bertz, L. S. Suh, L. M. Ittner, p38 MAP kinase-mediated NMDA receptor-dependent suppression of hippocampal hypersynchrony in a mouse model of Alzheimer inverted question marks disease. *Acta Neuropathol. Commun.* **2**, 149 (2014).
41. S. Ippati, C. H. Stevens, L. M. Ittner, Y. D. Ke, Early transient neuronal CyclinD1 expression precedes atrophy in the frontal cortex of APP23 mice. *SM J. Neurol. Disord Stroke* **3**, 1015s4 (2017).
42. J. Folch *et al.*, Role of cell cycle re-entry in neurons: A common apoptotic mechanism of neuronal cell death. *Neurotox. Res.* **22**, 195–207 (2012).
43. N. H. Varvel *et al.*, Abeta oligomers induce neuronal cell cycle events in Alzheimer's disease. *J. Neurosci.* **28**, 10786–10793 (2008).
44. T. Arendt, L. Rödel, U. Gärtner, M. Holzer, Expression of the cyclin-dependent kinase inhibitor p16 in Alzheimer's disease. *Neuroreport* **7**, 3047–3049 (1996).
45. I. Vincent, G. Jicha, M. Rosado, D. W. Dickson, Aberrant expression of mitotic cdc2/cyclin B1 kinase in degenerating neurons of Alzheimer's disease brain. *J. Neurosci.* **17**, 3588–3598 (1997).
46. C. Maestre, M. Delgado-Esteban, J. C. Gomez-Sanchez, J. P. Bolaños, A. Almeida, Cdk5 phosphorylates Cdh1 and modulates cyclin B1 stability in excitotoxicity. *EMBO J.* **27**, 2736–2745 (2008).
47. E. Barrio-Alonso, A. Hernández-Vivanco, C. C. Walton, G. Perea, J. M. Frade, Cell cycle reentry triggers hyperploidy and synaptic dysfunction followed by delayed cell death in differentiated cortical neurons. *Sci. Rep.* **8**, 14316 (2018).
48. Y. Negis, A. Karabay, Expression of cell cycle proteins in cortical neurons-Correlation with glutamate-induced neurotoxicity. *Biofactors* **42**, 358–367 (2016).
49. Y. Negis, A. Y. Unal, S. Korulu, A. Karabay, Cell cycle markers have different expression and localization patterns in neuron-like PC12 cells and primary hippocampal neurons. *Neurosci. Lett.* **496**, 135–140 (2011).
50. A. Copani *et al.*, Activation of cell-cycle-associated proteins in neuronal death: A mandatory or dispensable path? *Trends Neurosci.* **24**, 25–31 (2001).
51. A. W. Murray, Recycling the cell cycle: Cyclins revisited. *Cell* **116**, 221–234 (2004).
52. A. Hershko, A. Ciechanover, The ubiquitin system. *Annu. Rev. Biochem.* **67**, 425–479 (1998).
53. J. Lukas, J. Bartek, Cell division: The heart of the cycle. *Nature* **432**, 564–567 (2004).
54. R. Wäsch, F. R. Cross, APC-dependent proteolysis of the mitotic cyclin Clb2 is essential for mitotic exit. *Nature* **418**, 556–562 (2002).
55. W. Wei *et al.*, Degradation of the SCF component Skp2 in cell-cycle phase G1 by the anaphase-promoting complex. *Nature* **428**, 194–198 (2004).
56. C. Penas, V. Ramachandran, N. G. Ayad, The APC/C ubiquitin ligase: From cell biology to tumorigenesis. *Front. Oncol.* **1**, 60 (2012).
57. W. Yao *et al.*, Cdh1-APC is involved in the differentiation of neural stem cells into neurons. *Neuroreport* **21**, 39–44 (2010).
58. A. Almeida, J. P. Bolaños, S. Moreno, Cdh1/Hct1-APC is essential for the survival of postmitotic neurons. *J. Neurosci.* **25**, 8115–8121 (2005).
59. A. Almeida, Regulation of APC/C-Cdh1 and its function in neuronal survival. *Mol. Neurobiol.* **46**, 547–554 (2012).
60. Y. A. Lam *et al.*, Inhibition of the ubiquitin-proteasome system in Alzheimer's disease. *Proc. Natl. Acad. Sci. U.S.A.* **97**, 9902–9906 (2000).
61. Y. A. Sulistio, K. Heese, The ubiquitin-proteasome system and molecular chaperone deregulation in Alzheimer's disease. *Mol. Neurobiol.* **53**, 905–931 (2016).
62. P. K. Jackson, Developmental neurobiology: A destructive switch for neurons. *Nature* **442**, 365–366 (2006).
63. L. Krenning, F. M. Feringa, I. A. Shaltiel, J. van den Berg, R. H. Medema, Transient activation of p53 in G2 phase is sufficient to induce senescence. *Mol. Cell* **55**, 59–72 (2014).
64. B. Pucci, M. Kasten, A. Giordano, Cell cycle and apoptosis. *Neoplasia* **2**, 291–299 (2000).
65. A. Deshpande, P. Sicinski, P. W. Hinds, Cyclins and cdk in development and cancer: A perspective. *Oncogene* **24**, 2909–2915 (2005).
66. G. Roué, V. Pichereau, H. Lincet, D. Colomer, B. Sola, Cyclin D1 mediates resistance to apoptosis through upregulation of molecular chaperones and consequent redistribution of cell death regulators. *Oncogene* **27**, 4909–4920 (2008).
67. Y. J. Choi *et al.*, D-cyclins repress apoptosis in hematopoietic cells by controlling death receptor Fas and its ligand FasL. *Dev. Cell* **30**, 255–267 (2014).
68. K. H. Vousden, p53: Death star. *Cell* **103**, 691–694 (2000).
69. T. Ohtsuka, H. Ryu, Y. A. Minamishima, A. Ryo, S. W. Lee, Modulation of p53 and p73 levels by cyclin G: Implication of a negative feedback regulation. *Oncogene* **22**, 1678–1687 (2003).
70. G. D. Grant, K. M. Kedziora, J. C. Limas, J. G. Cook, J. E. Purvis, Accurate delineation of cell cycle phase transitions in living cells with PIP-FUCCI. *Cell Cycle* **17**, 2496–2516 (2018).
71. A. Sakaue-Sawano *et al.*, Genetically encoded tools for optical dissection of the mammalian cell cycle. *Mol. Cell* **68**, 626–640.e5 (2017).
72. B. T. Bajar *et al.*, Fluorescent indicators for simultaneous reporting of all four cell cycle phases. *Nat. Methods* **13**, 993–996 (2016).
73. S. Kügler, E. Kilic, M. Bähr, Human synapsin 1 gene promoter confers highly neuron-specific long-term transgene expression from an adenoviral vector in the adult rat brain depending on the transduced area. *Gene Ther.* **10**, 337–347 (2003).
74. A. E. Harasta *et al.*, Septal glucagon-like peptide 1 receptor expression determines suppression of cocaine-induced behavior. *Neuropsychopharmacology* **40**, 1969–1978 (2015).
75. T. Fath, Y. D. Ke, P. Gunning, J. Götz, L. M. Ittner, Primary support cultures of hippocampal and substantia nigra neurons. *Nat. Protoc.* **4**, 78–85 (2009).
76. W. B. Stine Jr, K. N. Dahlgren, G. A. Krafft, M. J. LaDu, In vitro characterization of conditions for amyloid-beta peptide oligomerization and fibrillogenesis. *J. Biol. Chem.* **278**, 11612–11622 (2003).
77. Y. D. Ke *et al.*, Short-term suppression of A315T mutant human TDP-43 expression improves functional deficits in a novel inducible transgenic mouse model of FTL-TDP and ALS. *Acta Neuropathol.* **130**, 661–678 (2015).
78. A. Barca *et al.*, Responsiveness of carnitine homeostasis genes in the pancreas and brain of streptozotocin-treated mice exposed to dietary carnitine. *Int. J. Mol. Sci.* **19**, 1713 (2018).
79. L. M. Ittner, D. Koller, R. Muff, J. A. Fischer, W. Born, The N-terminal extracellular domain 23–60 of the calcitonin receptor-like receptor in chimeras with the parathyroid hormone receptor mediates association with receptor activity-modifying protein 1. *Biochemistry* **44**, 5749–5754 (2005).
80. A. Barca *et al.*, Carnitine modulates the Sp1-Slc31a1/Ctr1 copper-sensing system and influences copper homeostasis in murine CNS-derived cells. *Am. J. Physiol. Cell Physiol.* **316**, C235–C245 (2019).
81. M. Bi *et al.*, Tau exacerbates excitotoxic brain damage in an animal model of stroke. *Nat. Commun.* **8**, 473 (2017).
82. G. von Jonquieres *et al.*, Glial promoter selectivity following AAV-delivery to the immature brain. *PLoS One* **8**, e65646 (2013).
83. A. van Hummel *et al.*, Selective spatiotemporal vulnerability of central nervous system neurons to pathologic TAR DNA-binding protein 43 in aged transgenic mice. *Am. J. Pathol.* **188**, 1447–1456 (2018).